communications earth & environment

A Nature Portfolio journal

Article

https://doi.org/10.1038/s43247-025-02571-z

Molybdenum isotope fractionations between ferromanganese oxides and seawater influenced ancient sedimentary isotopic signatures

Check for updates

Mengchun Cao[1], Guang-Yi Wei[1] ✉, Feifei Zhang[1], Xiangwen Ren[2], Xuefa Shi[2], Yi-Bo Lin[1], Tao Li[3], Sihui Chen[1], Hong-Fei Ling[1] & Jian Cao[1]

The use of molybdenum isotopes (δ^{98}Mo) as a paleo-redox proxy requires quantifications of fluxes and isotopic fractionations in each molybdenum sink. However, no systematic tests on δ^{98}Mo variations in different oxic sediments have been made due to limitations of analytical precision and sample number in pioneering studies. Here, we present the δ^{98}Mo data of ferromanganese nodules sampled at various global basins, which exhibit large variations from −0.95‰ to −0.51‰ with appreciable negative correlations between δ^{98}Mo and manganese–iron ratios. Diagenetic nodules, experiencing dissolution and re-precipitation of manganese oxides in marine sediments, have lower δ^{98}Mo by ~0.3‰ and higher molybdenum contents relative to hydrogenetic nodules. We suggest that changes in relative proportions of manganese and iron oxides and early diagenesis of marine sediments likely influence overall molybdenum isotope fractionations in oxic sinks. Hence, evolution of ancient marine manganese and iron cycles can influence sedimentary δ^{98}Mo signatures, especially in low-oxygen Precambrian oceans.

Molybdenum (Mo) and its isotope compositions (δ^{98}Mo, modified relative to NIST SRM 3134 = +0.25‰) have been widely used to reconstruct the average oxygenation level of global ocean through Earth's history, attributed to the long resident time of Mo in the global ocean (e.g., 0.44–0.7 Myr in modern oceans)[1] and large Mo isotope fractionations occurring between oxic-suboxic sediments and seawater[2–4]. Although δ^{98}Mo of global seawater may have been homogeneous throughout most of geological time, the records in sedimentary rocks (e.g., shales) are highly variable due to the different isotopic fractionations between sediments and seawater, controlled by local seawater redox and depositional environments[5–9]. Depending on the distinct isotopic fractionations and fluxes, at steady-state, δ^{98}Mo and Mo concentration of global seawater can be determined by the relative proportions of Mo sinks in different types of sediments, when the fluxes and isotopes of Mo source are relatively constant[10]. Due to limited Mo isotopic fractionations and high Mo burial rates in strongly euxinic sediments, high δ^{98}Mo and Mo concentration of global seawater are ultimately caused by abundant Mo burial in oxic sediments, reflecting decreases in global euxinic seafloor area[11,12]. For instance, the rise to modern seawater δ^{98}Mo signatures (~+2.34‰) in sedimentary rocks was proposed to represent the establishment of modern-like oxygen levels in early Cambrian oceans[11]. However, such high δ^{98}Mo values have been occasionally documented in sedimentary rocks through the Proterozoic[13–15], during which other geochemical indices suggest extensive anoxic conditions, and instead interpreted as changes in local marine Mo cycles. Meanwhile, decreases in ancient seawater δ^{98}Mo can be induced by lower Mn burial rates, instead of expanded euxinic seafloor, for instance, during the Cretaceous OAE2 (ref. 16). Taken together, there are still large debates on whether changes in seawater δ^{98}Mo indicates substantially varying proportions of global seafloor redox conditions.

Compared to studies of anoxic Mo sinks[5–8,17–20], the kind and extent of Mo isotopic fractionations in oxic sinks and their effects on global marine sedimentary δ^{98}Mo signals are relatively understated in previous work due to the limited data for modern Fe-Mn oxides[5,6]. The pioneering studies concentrated on investigations of the surface layer of ferromanganese crusts

[1]State Key Laboratory of Critical Earth Material Cycling and Mineral Deposits, School of Earth Sciences and Engineering and Frontiers Science Center for Critical Earth Material Cycling, Nanjing University, Nanjing, China. [2]Key Laboratory of Marine Geology and Metallogeny, First Institute of Oceanography, Ministry of Natural Resources, Qingdao, China. [3]State Key Laboratory of Palaeobiology and Stratigraphy, Nanjing Institute of Geology and Palaeontology, Chinese Academyof Sciences, Nanjing, China. ✉e-mail: guangyiwei@nju.edu.cn

and bulk nodules that potentially represent modern deposits of oxides and have relatively uniform δ^{98}Mo values with a small sample number (δ^{98}Mo = –0.7‰ ± 0.1‰, 1 SD, n = 8)[5,6]. Additionally, the interpretations of the controlling factors on δ^{98}Mo signatures in Fe-Mn oxides and their potential influence on marine Mo cycles have not been fully tested in natural sedimentary records, due to the lack of ample samples and systematic investigations of their geochemical compositions. A recent study analyzed different types of hydrothermal oxides, showing large δ^{98}Mo differences in Fe-oxides and Mn-oxides[21], which is consistent with the results from synthetic experiments[22–24]. Nevertheless, uncertainties remain when considering the source of Mo in hydrothermal systems and its reliability for representing Mo sink in oxic pelagic sediments[21]. Here, we revisit Mo isotope compositions of marine oxic Mo sinks and their effects on global marine Mo isotopic mass balance by systematically investigating the elemental and isotopic signatures of ferromanganese nodules—one of the major Mn-Fe precipitates in oxic marine seafloor. Ferromanganese nodules in different oceanic basins are studied to uncover the depositional processes that affect Mo isotope fractionations between oxic sediments and seawater (Fig. 1). Comparing δ^{98}Mo data from ferromanganese nodules in this study and other types of oxides (e.g., ferromanganese crust, hydrothermal oxides), we suggest that the Mo burial flux and isotopic fractionation between oxic sediments and seawater are not invariant, but closely related to the evolution of marine Fe and Mn cycles. In this view, the overall extent of global marine oxygenation based on Mo isotope records should be re-examined, especially during the Precambrian with low baseline of atmospheric and marine oxygen levels.

Large Mo isotope variations of hydrogenetic and diagenetic nodules

Both full digestion and partial leaching protocols (see Materials and methods) have been applied for geochemical analyses of ferromanganese oxides in previous studies for different metal isotope systems. For instance, full digestion for Mo, V and Ce isotopes[5,25,26], and partial leaching using HCl for Mo, Tl, and U isotopes[6,27,28]. The studied ferromanganese nodules contain appreciable detrital precipitates (e.g., aluminosilicates) based on XRD analysis[29], which is also consistent with high Al contents of bulk samples (3.2% ± 0.7%, 1σ) in this study (Supplementary Fig. 1). In contrast, although HCl can likely dissolve parts of detrital materials, leached samples exhibit appreciably decreased Al contents (1.8% ± 0.5%, 1σ) relative to bulk samples (Supplementary Fig. 1). In general, the ferromanganese nodules after full digestion and partial leaching show similar δ^{98}Mo compositions due to low Mo contents in continental detrital minerals relative to ferromanganese oxides[6], however, the $\delta^{98}Mo_{bulk}$ values of a few samples are appreciably higher than $\delta^{98}Mo_{leach}$ in this study (Supplementary Fig. 1). Given high Mo contents of the studied nodules (~260 ppm to 470 ppm), a considerable amount of additional Mo with high δ^{98}Mo (e.g., 30 ppm, +1.0‰) is likely required to explain an offset of ~0.1‰ between $\delta^{98}Mo_{bulk}$ and $\delta^{98}Mo_{leach}$. With a few uncertainties, we suggest that this difference may be owing to the preferential dissolution of seafloor materials marked by high Mo contents and δ^{98}Mo values[6], such as organic matter-rich marine sediments or phosphates in bulk samples[30–32]. Meanwhile, the full digestion of bulk samples would also lead to more additions of Fe, along with other metal elements, from silicate minerals (e.g., Fe-bearing clays), hampering the investigations of relationships between δ^{98}Mo and these elements. Hence, in order to better extract the seawater information, all the geochemical data discussed below are derived from HCl leaching results, which are also comparable to previous study of ferromanganese crusts[6].

Marine ferromanganese nodules precipitating throughout the oceans are commonly identified as hydrogenetic, diagenetic, or hydrothermal in origin, reflecting their depositional environments and modes of accretion[33–35]. The hydrogenetic nodules are generally formed via the direct oxidation of dissolved Fe^{2+} and Mn^{2+} in oxygen-sufficient seawater, and then the accretion of amorphous or cryptocrystalline Fe-oxyhydroxide and Mn-oxide colloids around a nucleus[35]. By contrast, the formation of diagenetic nodules occurs within the sediment upper porewater or at the sediment-water interface on the deep seafloor, reflecting the dissolution of Mn-oxides and reprecipitation of more crystallized phyllomanganates[35]. In this study, multiple geochemical approaches were used to discriminate the types of the studied nodules, including rare earth elements (REE) and high-field strength elements (Fig. 2)[33,34]. Most of the studied nodules are hydrogenetic with relatively low Mn/Fe ratios and Cu, Ni, Co contents, and high REE contents along with a significantly positive Ce anomaly (Ce/Ce* defined as the relative enrichments or depletions in Ce relative to other REE). In contrast, other five nodules are marked by considerably high Mn/Fe ratios, low REE contents, seawater-like REE patterns, indicative of a diagenetic origin following dissolution and reprecipitation of oxides through the suboxic sediment column, and elemental exchanges with bottom seawater[33] (Fig. 2). Despite minor discrepancies among different geochemical classification approaches (Fig. 2), the compositions of these five nodules are clearly distinct from those of typical hydrogenetic and hydrothermal nodules, reliably indicating diagenetic overprinting on their geochemical signatures. Overall, we conservatively identify the origins for different

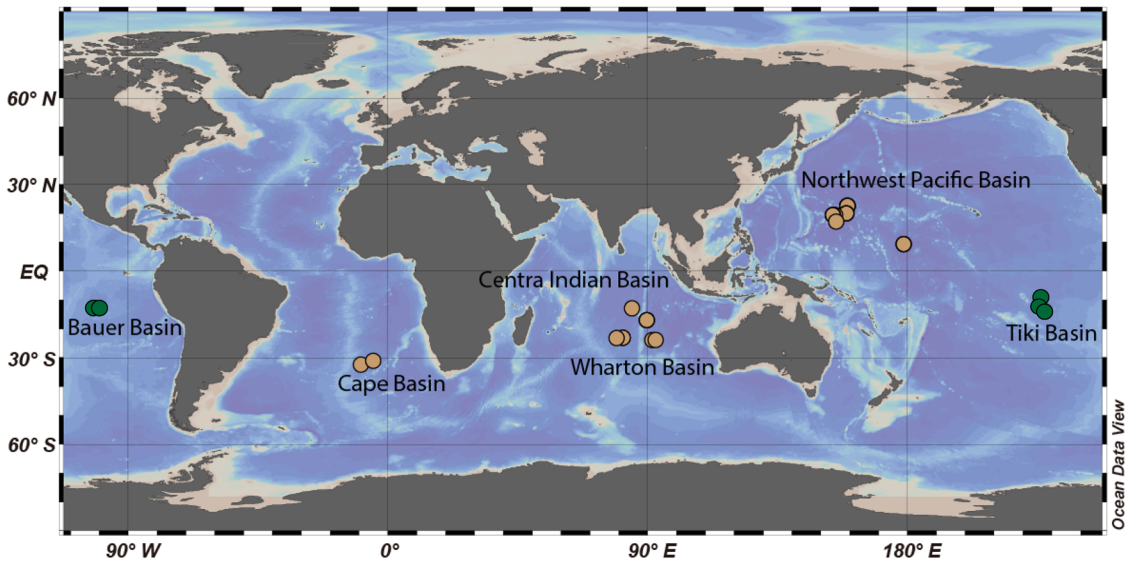

Fig. 1 | Locations of sites for the studied ferromanganese nodules in different oceanic basins. The background map of global ocean is from Ocean Data View (https://odv.awi.de). The tan points denote the hydrogenic origin and the green points denote the diagenetic origin for the studied nodules.

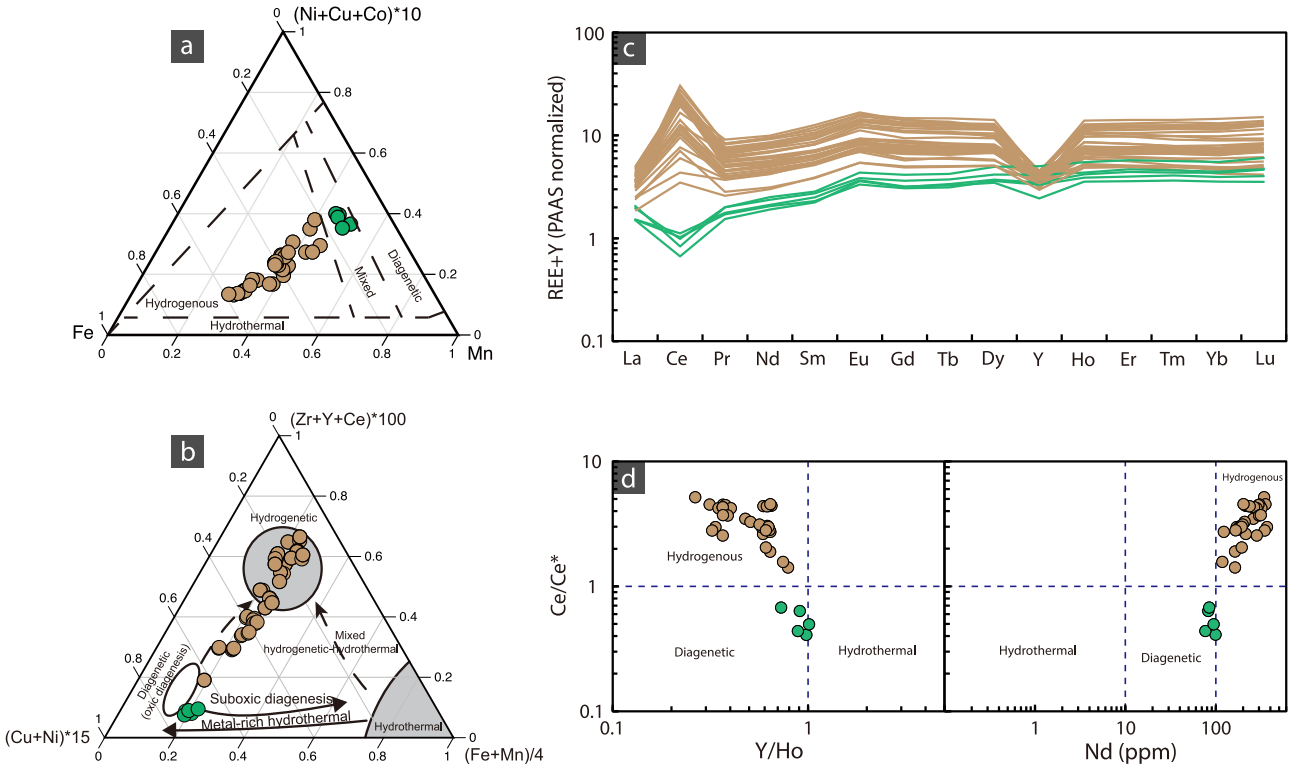

Fig. 2 | Discrimination of nodule genesis using high field strength elements and rare earth elements. a, **b** using metal element indicator[34]; **c**, **d** using rare earth elements and Y indicator[33]. The Ce anomaly (Ce/Ce*) is calculated using the equation $Ce/Ce^* = Ce_n/(Pr_n^2/Nd_n)$, where *n* denotes normalization of each concentration against the post-Archean Australian shale (PAAS)[51].

nodules based on combined results from major/trace elements and rare earth elements. Additionally, the diagenetic nodules have more phyllomanganate minerals relative to hydrogenetic nodules, based on XRD analysis of the identical sample set in previous study[29]. No hydrothermally originated nodules are identified in this study. Hence, Mo isotope compositions of different types of nodules are individually discussed below.

Previous studies of surface layers of ferromanganese crusts and bulk nodules showed overall Mo isotope fractionations of −3.0‰ between oxides and recent seawater ($\delta^{98}Mo_{oxides} \approx -0.7 \pm 0.1$‰, 1 SD, $n = 8$)[5,6]. Considering that external analytical reproducibility in the early studies was ~0.1‰, changes in δ^{98}Mo values of ferromanganese crust surface layers are relatively limited with a small sample number[6]. Although the whole profile of an Atlantic ferromanganese crust shows appreciably lower δ^{98}Mo signatures (−0.9‰ to −0.8‰), such low values only occur during ca. 62–7 Ma, while δ^{98}Mo values of sub-surficial layers (−0.6‰ ~ −0.5‰) are close to those of Atlantic nodule standard (Nod-A-1), surface layers of other crusts, and the Pacific crust profile[6] (Fig. 3a). By comparison, the hydrogenetic and diagenetic nodules in this study exhibit appreciably larger δ^{98}Mo ranges from −0.95‰ to −0.51‰ and a clear negative correlation between δ^{98}Mo and Mn/Fe ($r = -0.76$ for all the nodules and $r = -0.63$ for only hydrogenetic nodules in this study). Further, the δ^{98}Mo of diagenetic nodules (−0.95‰ to −0.71‰) are systematically lower than those of hydrogenetic nodules (−0.77‰ to −0.51‰) (p value $= 2.37 \times 10^{-7}$ in Student *t-test*), and previously reported data for crusts (Fig. 3a). The notable correlation between $\delta^{98}Mo_{leach}$ and Mn/Fe observed in this study suggest that Mo isotope compositions of ferromanganese nodules are not homogeneous and likely affected by their mineralogy. The hydrogenetic nodules, marked by relatively low Mn/Fe, comprise larger proportions of primary Fe-(oxyhydr) oxides (e.g., amorphous ferrihydrite and cryptocrystalline Fe-vernadite), whereas diagenetic nodules are dominated by phyllomanganates due to recycling of Mn with sediment piles[35]. Previous studies have demonstrated that Fe-(oxyhydr)oxides can substantially adsorb isotopically light Mo from seawater but show distinctly smaller isotopic fractionations ($\Delta^{98}Mo_{Fe\text{-}oxide\text{-}seawater} = -0.8$‰ to −2.2‰) and lower Mo concentrations relative to Mn-oxides[9,22,36]. Hence, the correlation between δ^{98}Mo and Mn/Fe of the studied samples is suggested as a result of mixing Fe-(oxyhydr) oxide and Mn-oxide minerals in nodules. Further, diagenetic nodules show appreciably larger Mo isotope fractionations than experimentally constrained fractionations in synthetic Mn oxides, with higher Mo contents relative to hydrogenetic nodules (314.6 ± 34.1 ppm for hydrogenetic and 437.9 ± 29.4 ppm for diagenetic nodules, 1σ) (Fig. 3b), likely reflecting substantial adsorption of additional Mo with light isotopes from suboxic pore water in deeper sediment profiles, more rapid growth rates of diagenetic nodules[35,37], or larger distribution coefficient of Mo in Mn-oxides compared with Fe-(oxyhydr)oxides[36].

Heterogeneous Mo isotope signatures in different types of ferromanganese oxides

In this study, the ferromanganese nodules from different basins in modern global ocean exhibit large ranges of δ^{98}Mo (−0.95‰ to −0.51‰) and Mo content (260.0–471.3 ppm), which are highly related to the Mn/Fe ratios (i.e., mineralogy and precipitating environments) of nodules. The pioneering work has observed appreciable variations of δ^{98}Mo in surface layers of ferromanganese crusts, while variations of Mo isotope fractionation are interpreted to be related to the species of Mo^{6+} in the oceans and then the adsorption efficiency of Mo in Fe- and Mn- oxides[5,6]. As the studies of surface layers of ferromanganese crusts did not present Mn/Fe data of the samples[6], the effects of relative proportions of Fe- and Mn-oxides on their δ^{98}Mo signatures have not been examined. Nevertheless, the observation of larger δ^{98}Mo ranges and close correlations between δ^{98}Mo and Mn/Fe in the studied ferromanganese nodules bolsters the different roles of Fe- and Mn-oxides in regulating overall Mo isotope fractionations between oxides and seawater, which is supported by the results of laboratory synthetic experiments[22,23,36]. Additionally, analogous to the formation of diagenetic nodules, the dissolution of pre-formed Mn oxides in suboxic deeper pore waters, and subsequent re-oxidation after the dissolved Mn diffuses

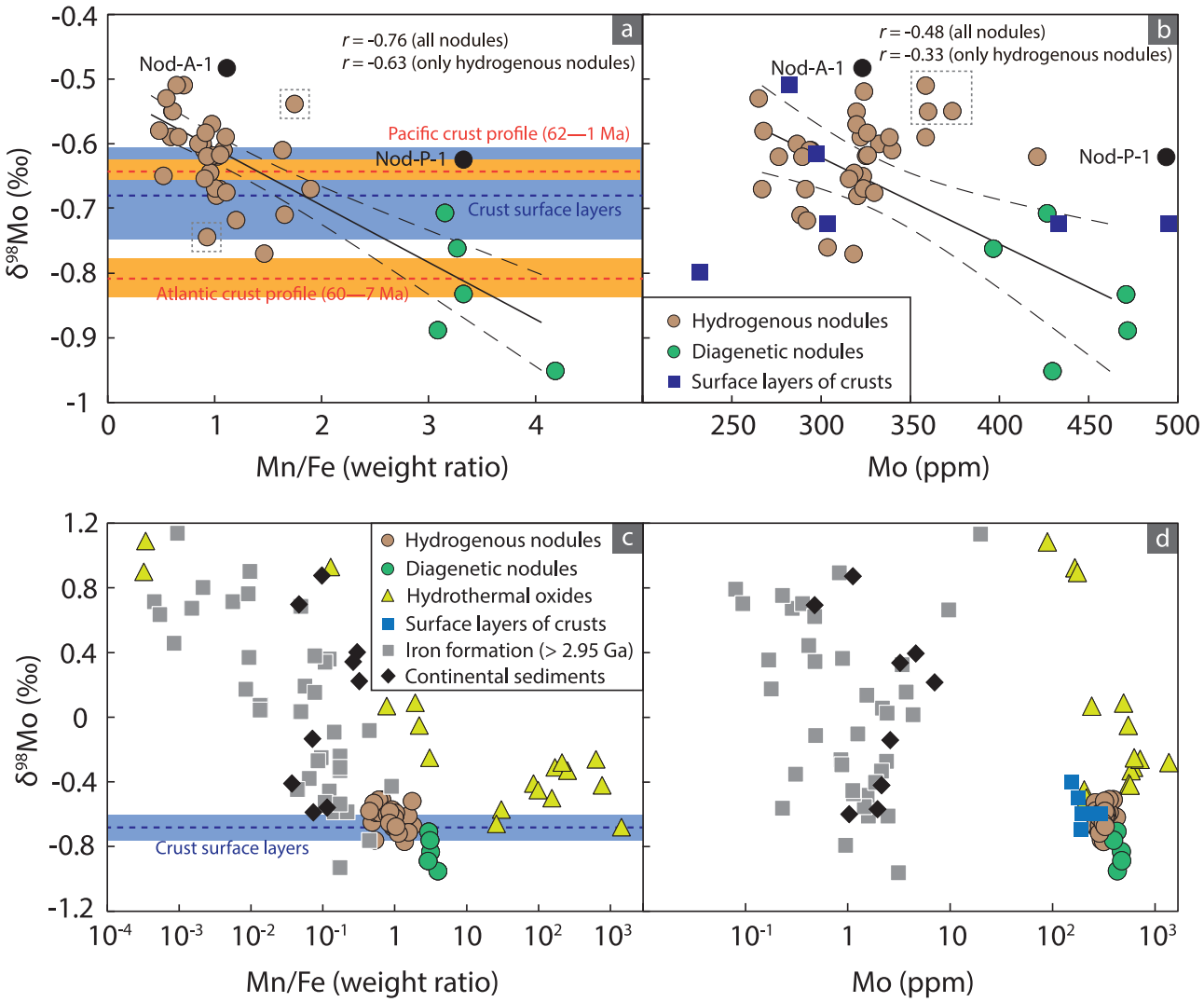

Fig. 3 | Cross-plots of δ^{98}Mo vs. Mn/Fe ratio and Mo content for different types of ferromanganese oxides. In **a** we plot the nodule samples and USGS nodule standards (Nod-A-1 and Nod-P-1) in this study. As previous studies did not present Mn/Fe data, the dashed lines and shadowed areas represent the average Mo isotopic fractionations and their ranges between ferromanganese crusts or nodules, and seawater[6,23]. In **c**, **d** the δ^{98}Mo data of modern hydrothermal oxides, Mn-rich continental anoxic sediments, and the Archean iron formations are compiled from refs. 9,21,40. The *r* values in **a**, **b** denote the trimmed coefficients of determination of the correlations (exclusion of outliers in the dashed squares).

upwards to relatively oxic upper sediments (i.e., recycling of Mn oxides through the sediment column) can lead to the accumulation of more isotopically lighter Mo in diagenetic Mn oxides near the bottom water-sediment interface. This process is likely pervasive under fluctuating redox conditions of bottom seawater ranging between suboxic ($[O_2]$ <10 μM) and hypoxic ($[O_2]$ <61 μM) levels, during which only recycling of Mn oxides remains active[38,39]. We further compiled δ^{98}Mo and elemental data of hydrothermal oxides and the Archean iron formations in previous studies[21,40], and compared them to ferromanganese nodules in this study (Fig. 3c, d). Despite the hydrothermal oxides showing appreciable correlations between δ^{98}Mo and Mn/Fe, their δ^{98}Mo values and Mo contents are systematically higher than those of ferromanganese crusts and nodules (Fig. 3c, d), even considering those oxides with significantly high Mn/Fe ratios (>100). This observation may suggest that the hydrothermal oxides, especially Mn-oxides may not represent typical open-marine depositional environment, or adsorb non-marine sourced Mo in hydrothermal systems[21]. In contrast, the Archean iron formations exhibit much lower Mn/Fe and Mo contents, but high δ^{98}Mo values (Fig. 3c, d), indicative of less Mo removal via Mn oxides, and overall low Archean oxygenation levels. The correlations between δ^{98}Mo values vs. Mn/Fe ratios and Mo contents in these Archean iron formations also suggest that the Mo isotope fractionations in ancient oceans are determined by formation of Mn oxides.

Despite the uncertainties on whether ferromanganese crusts and nodules are sufficiently large in mass to be the dominant Mo sink, authigenic Fe- and Mn-oxides in marine pelagic sediments can be a significant sink for Mo via the association with grain coatings and micronodules in these sediments[6,41,42]. The Mn/Fe ratios of authigenic oxides in their associated marine sediments can be comparable to those of ferromanganese nodules, and diagenetic remobilization within the sediments can increase Mn/Fe ratios and Mo contents in the oxides[42]. In this view, the relative proportions of co-precipitating Fe- and Mn-oxides in marine pelagic sediments may have influenced the average Mo isotope fractionations between the oxic sink and seawater on a global scale. Additionally, during the early diagenetic remobilization (i.e., recycling of Mn oxides within sediment piles), increased Mn/Fe ratios of authigenic oxides in sediments may remove more Mo from the bottom seawater, supported by the dominant role of Mn-oxide in binding Mo in pelagic sediments[42,43]. Thus, the Mo isotope offsets between oxides in marine pelagic sediments and bottom seawater are likely larger than those of hydrogenous crusts and nodules.

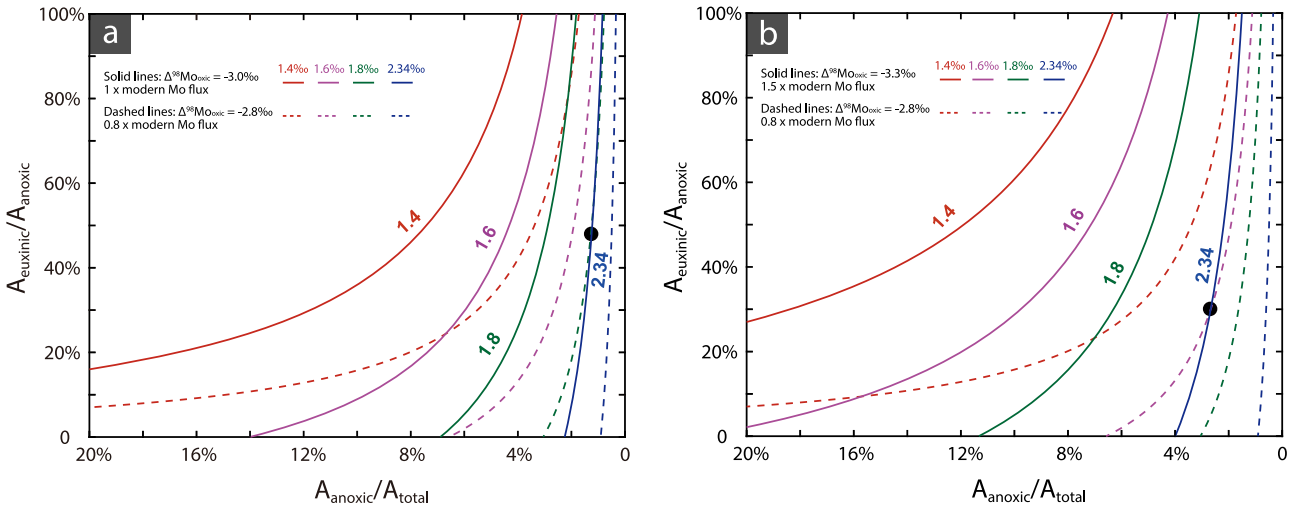

Fig. 4 | Mo mass balance model showing changes in global seawater δ^{98}Mo as functions of seafloor areas with different redox conditions. a Comparisons of modern ocean (solid lines with Δ_{oxic} = −3.0‰) and estimated Fe cycling active ocean (dashed lines with Δ_{oxic} = −2.8‰) with different Mo isotope fractionations and fluxes in the oxic sink. **b** Comparisons of estimated Mn cycling active (solid lines with Δ_{oxic} = −3.3‰) and Fe cycling active oceans (dashed lines with Δ_{oxic} = −2.8‰). Under the typical framework of Mo isotope budgets in the modern ocean, the removal of Mo from seawater mainly occurred under strongly euxinic conditions ($[H_2S]$ > 11 μM) with the lowest isotopic fractionation but high burial flux (subscripted euxinic). In contrast, the removal of Mo in oxic sediments occurred under oxic conditions with $[O_2]$ higher than 10 μM associated with high isotopic fractionation but low burial flux, following the formation of Mn oxides in global pelagic sediments (subscripted oxic). The intermediate sink for Mo includes a large range of redox conditions [i.e., suboxic (0 <$[O_2]$ <10 μM), anoxic ($[O_2]$ = 0 μM, $[H_2S]$ = 0 μM), and weak euxinic conditions ($[O_2]$ = 0 μM, 0 <$[H_2S]$ <11 μM)], which is uniformly defined as a "anoxic" condition (subscripted anoxic) in this study. The detailed descriptions of model and selected parameters are presented in the Supplementary Methods and Table 1.

The potential effects of Mo isotope compositions in ferromanganese oxides on sedimentary δ^{98}Mo records in deep time

Oceanic Mo isotope mass balance suggests gradual increases in seawater δ^{98}Mo accompanying with decreased Mo burial in euxinic sinks, and namely elevated Mo burial in the oxic sinks (i.e., Fe- and Mn-oxides in marine sediments), which is used to estimate the area of oxic versus euxinic seafloor areas in the global ocean[10]. However, when the seafloor areas of each Mo sink under different redox conditions are invariant, seawater δ^{98}Mo can also be influenced by changes in isotopic fractionations in each sink. For instance, decreased burial flux of Mn-oxides when bottom seawater is suboxic may diminish Mo burial proportions in oxic marine sediments at the global scale, and drive global seawater δ^{98}Mo towards to low values without expansion of euxinic seafloor during Cretaceous OAE2[16]. Similarly, the transition from Fe oxide to Mn oxide formation dominated in global marine sediments, meaning more Mo burial in Mn-oxide minerals may have significantly increased seawater δ^{98}Mo without requirements of decreased euxinic seafloor. Here, we use a Mo isotope mass balance model to reproduce the seawater δ^{98}Mo variations as the function of the seafloor areas with different redox states (Fig. 4) (see Supplementary Methods for model descriptions and parameters). In the model, we compare the effects of Mo burial rates and isotopic fractionations during the formation of different oxides on global seawater δ^{98}Mo. The average isotopic fractionation associated with the natural oxic Mo sink in the modern ocean is generally assumed as −3.0‰, based on previous assessments of global Mo burial with Fe and Mn oxides on the oxic seafloor[6–8]. Building on the observed relationship between δ^{98}Mo and Mn/Fe from the studied ferromanganese nodules, we adopt a fractionation value of −2.8‰ to represent Fe oxide-dominated conditions in suboxic marine sediments (i.e., low Mn/Fe ratios of the oxic sediments), and −3.3‰ to represent Mn oxide-dominated conditions (i.e., high Mn/Fe ratios of the oxic sediments). It should be noted that the value of −3.3‰ is appreciably larger than experimentally observed Mo isotope fractionations between Mn oxide and solution (−2.4‰ to −2.9‰)[23,24]. This discrepancy is proposed to result from recycling of Mn oxides through the sediment piles during early diagenesis, a process analogous to the formation of diagenetic nodules[39,41,42]. This interpretation is consistent with the observation that δ^{98}Mo values of surface layers of ferromanganese crusts remain slightly lower than those of synthetic δ-MnO_2 under the seawater condition[6,23,24], partly suggesting the potential diagenetic effects during the deposition and burial of ferromanganese crusts. Additionally, in the model (Fig. 4), the burial rates of Mo in Mn oxide-rich marine sediments are assumed to be higher than those in Fe oxide-rich sediments, as Mn oxides play a dominant role in removing Mo in global marine sediments[41–43]. The results of the mass balance models show clear shifts of seawater δ^{98}Mo accompanying the variations of isotopic fractionations between oxic sediments and seawater. A notable increase in seawater δ^{98}Mo from 1.8‰ to 2.34‰ can be observed when global oxide-dominated Mo sink transfers from Fe-oxide to mixing Fe- and Mn-oxides (e.g., modern ocean conditions), even with no changes in anoxic and euxinic seafloor areas (Fig. 4a). Moreover, our model results suggest that the amplification of seawater δ^{98}Mo increases is more prominent when Mn-oxides become to dominate the oxic sink of Mo (from 1.6‰ to 2.34‰ in Fig. 4b).

Changes in the proportions of the burial of Fe- and Mn-oxides, and enhanced recycling of Mn oxides under suboxic–hypoxic redox conditions may have affected the Precambrian δ^{98}Mo records when baseline of atmospheric and marine oxygenation levels was substantially lower than present time, especially in the late Archean and late Neoproterozoic (Fig. 5a). Due to the differences in the redox potential for Fe and Mn, Fe^{2+} is preferentially oxidized in the ocean prior to Mn^{2+}, when marine oxygen gradually increases[38,44]. The Archean oceans were dominated by overall anoxic and ferruginous conditions, thus the formation of Fe oxides in marine sediments was more prevalent relative to Mn oxides when oxygenation levels of global ocean gradually increased[45,46], leading to persistently low δ^{98}Mo signals in marine sedimentary records during the peak of banded iron formations (Fig. 5a). Accordingly, increased sedimentary δ^{98}Mo signals during the Archean–Paleoproterozoic transition can be attributed to enhanced burial of Mn oxides in global pelagic sediments (Fig. 5a), without the requirement of decreased anoxic and euxinic seafloor area. The temporal distributions of banded iron formations and sediment-hosted Mn ores from the late Archean to early

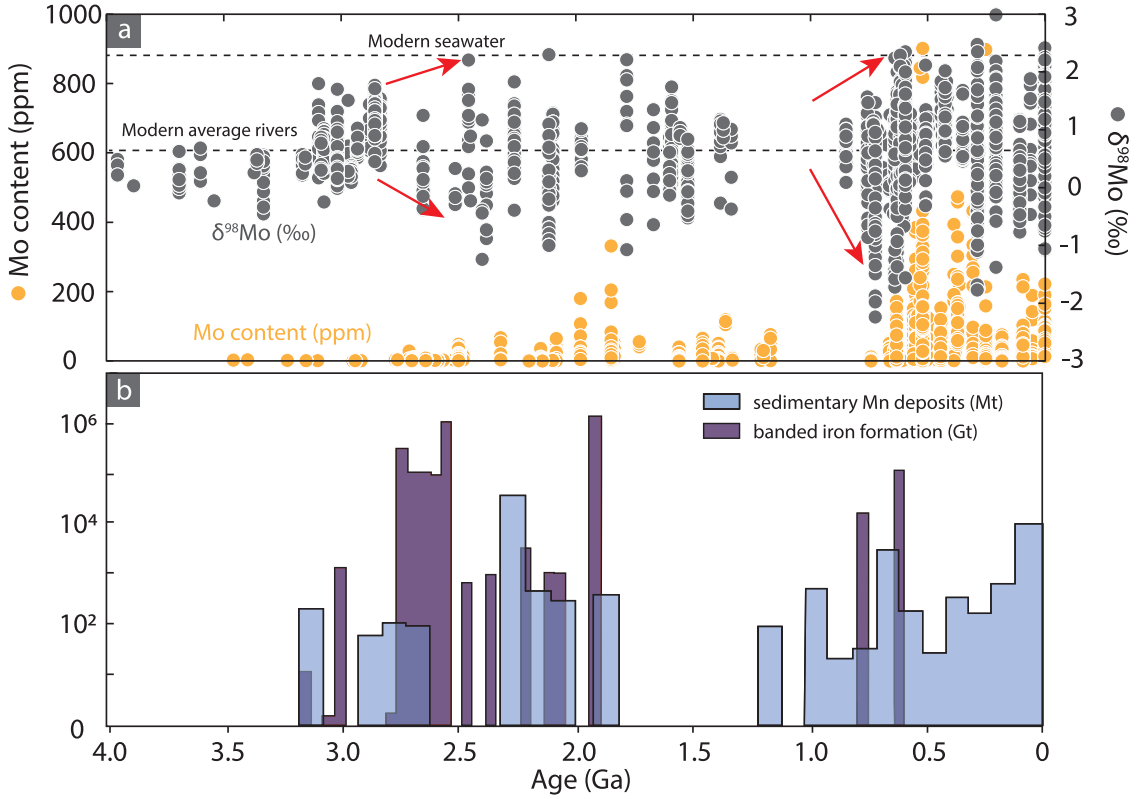

Fig. 5 | Mo isotope records in shales and abundance distributions of banded iron formations and sedimentary Mn deposits through geological time. a Marine sedimentary records of Mo isotopes throughout geological time. **b** Temporal changes in distributions of banded iron formations and sedimentary Mn deposits. In **a** the dashed line in represents the δ^{98}Mo values of modern seawater and average rivers[10]. Red arrows denote the increased occurrence of positive and negative δ^{98}Mo signatures following the enhanced marine Mn cycle. The δ^{98}Mo data of shales are modified from ref. 14. The distributions of banded iron formations and sedimentary Mn deposits are modified from refs. 45,46.

Paleoproterozoic also support the conversions from Fe active to Mn active cycles following the stepwise oxidation of Precambrian oceans (Fig. 5b). The transitions to substantial formation of Mn oxides are also observed from the late Neoproterozoic to early Paleozoic due to the accumulation of dissolved Mn in seawater under suboxic conditions (i.e., $[O_2]$ <10 μM defined as a "manganous condition")[47]. Thus, the substantially increased sedimentary δ^{98}Mo signals from the latest Neoproterozoic can be amplified due to increases in Mn oxide formation as a dominant Mo sink on the seafloor, when global seawater started to mark with hypoxic conditions ($[O_2] > 10$ μM) (Fig. 5a). In this light, the preservation of near-modern seawater δ^{98}Mo signals during the Neoproterozoic and Paleozoic transition does not necessarily indicate a rise in global ocean oxygenation to near-modern levels. Although transitions of marine Fe and Mn cycles imply the gradual increases in seawater oxygen, the average extent to global marine oxygenation, evaluated from high δ^{98}Mo values in sedimentary records, could still be low (e.g., hypoxic conditions). Conversely, oceanic deoxygenation during the Phanerozoic may also reduce global seawater δ^{98}Mo by decreasing Mn oxide formation and more Mo removal via Fe oxide in marine sediments, which do not necessarily require the expansion of euxinic conditions[3]. Additionally, analogous to the case on more negative δ^{98}Mo in diagenetic nodules, active marine Mn cycles when seawater redox states vary between suboxic and hypoxic conditions[38] may also account for more distributions of negative δ^{98}Mo signatures in sedimentary records from the early Paleoproterozoic and late Neoproterozoic (Fig. 5a), due to the recycling of isotopically light Mo from Mn-oxides during early diagenesis. Thus, more distributions of negative δ^{98}Mo in shales may reflect the expansion of suboxic–hypoxic conditions, rather than euxinic conditions.

Conclusions

This study provided a systematic investigation of δ^{98}Mo signatures in the marine ferromanganese nodules from different oceanic basins to better explore Mo isotope fractionations between oxic sediments and seawater and their effects on ancient marine Mo isotope cycles. The δ^{98}Mo values of nodules exhibit considerably larger variation ranges relative to those of surface layers of ferromanganese crusts in the pioneering research, which are tightly related to Mn/Fe ratios of nodules. Additionally, diagenetic nodules, comprising more phyllomanganates, have lower δ^{98}Mo values and higher Mo contents relative to hydrogenetic nodules, suggesting that dissolution and re-precipitation of Mn-oxides within marine sediments may lead to larger Mo isotope fractionations between oxides and seawater. Accordingly, we propose that changes in relative proportions of authigenic Fe- and Mn-oxides preserved marine pelagic sediments may have influenced overall Mo isotope fractionations in oxic sink of global ocean. In this view, sedimentary δ^{98}Mo evolution through Earth's history, especially large δ^{98}Mo shifts during the Precambrian, is closely associated to changes in global marine Fe and Mn cycling.

Methods

Sampling

Thirty-nine nodule samples were collected from 18 sites in 6 basins in the Pacific, Indian, and Atlantic oceans (Fig. 1)[29], with detailed location information in the Supplementary Table 1. The collected nodules were formed with water depths ranging from 4271 m to 5629 m, whose structures were mainly spheroidal, joined spheroidal, and cauliflower-shaped. Based on previous XRD analysis, the minerals in the collected nodules are mainly composed of todorokite, phyllomanganate, vernadite, ferrihydrite, quartz, and phillipsite[29]. The samples for geochemical analyses were scraped from

the surface of each nodule to a depth of 1–2 mm and then ground into 200-mesh powders.

Geochemical analyses

The sample powders were analyzed for elemental and isotopic data using full digestion (with a subscript of "bulk") and partial leaching approaches (with a subscript of "leach"), respectively. For full digestion, mixing acids of HF + HNO_3 + HCl was used to dissolve both ferromanganese oxides and potential aluminosilicates in nodules. For partial dissolution of ferromanganese oxides, the bulk samples were leached with 6 M HCl overnight at room temperature following the previous studies of ferromanganese crusts and nodules[6,27]. The USGS geostandard Nod-A-1 was also treated using the 6 M HCl leaching approach. The above sample solutions were measured for major and trace elements using a Thermo Element XR ICP-MS at the Metal Isotope Geochemistry Lab in the Centre for Research and Education on Biological Evolution and Environment (CREBEE), Nanjing University. The OSIL seawater and USGS Nod-A-1 standards were analyzed to monitor the long-term instrument precision, which is typically better than 5% in this study.

For Mo isotope analysis, a ^{97}Mo–^{100}Mo double spike was used to calibrate the potential Mo isotope fractionation during the Mo separation and isotopic measurement. The sample-spike mixtures were purified using 0.8 mL TRU resin in an Eichrom 2 mL column, modified from the procedure in a previous study[48]. The purified Mo solution was analyzed for isotopic ratios using a Thermo Scientific Finnigan Neptune XT MC-ICP-MS associated with a CETAC Aridus III desolvating system at CREBEE, Nanjing University. The Mo isotope ratios are ultimately reported in standard delta (δ^{98}Mo) notation relative to the NIST SRM 3134 Mo standard using the equation below:

$$\delta^{98}\mathrm{Mo} = [(^{98}\mathrm{Mo}/^{95}\mathrm{Mo})_{\mathrm{sample}}/((^{98}\mathrm{Mo}/^{95}\mathrm{Mo})_{\mathrm{NIST\,3134}} \times 0.99975) - 1] \times 1000$$

Here, the δ^{98}Mo value of NIST SRM 3134 is defined as +0.25‰ to better compare with previously published Mo isotope data[49]. The long-term external reproducibility of analysis was assessed to be better than ±0.05‰ (2σ), based on repeated measurements of NIST SRM 3134 ($\delta^{98}Mo_{3134}$ = +0.25‰ ± 0.03‰ n = 30), OSIL seawater standard ($\delta^{98}Mo_{seawater}$ = +2.34‰ ± 0.04‰, n = 4) and USGS Nod-A-1 and Nod-P-1 manganese nodule standards ($\delta^{98}Mo_{Nod\text{-}A\text{-}1}$ = –0.48‰ ± 0.05‰, n = 2 and $\delta^{98}Mo_{Nod\text{-}P\text{-}1}$ = –0.62‰ ± 0.03‰, n = 4), consistent with recently published data[48,50].

Data availability

All data supporting the findings of this study are available within the paper and its Supplementary Information. The original geochemical data are presented in the Supplementary Table 2 and are publicly available at Zenodo (https://doi.org/10.5281/zenodo.15687982).

Code availability

Code for Mo isotope mass balance model (in MATLAB) is posted on Zenodo (https://doi.org/10.5281/zenodo.15687982).

Received: 7 February 2025; Accepted: 10 July 2025;
Published online: 18 July 2025

References

1. Miller, C. A., Peucker-Ehrenbrink, B., Walker, B. D. & Marcantonio, F. Re-assessing the surface cycling of molybdenum and rhenium. *Geochim. Cosmochim. Acta* **75**, 7146–7179 (2011).
2. Scott, C. et al. Tracing the stepwise oxygenation of the Proterozoic ocean. *Nature* **452**, 456–459 (2008).
3. Dickson, A. J. A molybdenum-isotope perspective on Phanerozoic deoxygenation events. *Nat. Geosci.* **10**, 721–726 (2017).
4. Wei, G.-Y. et al. Global marine redox evolution from the late Neoproterozoic to the early Paleozoic constrained by the integration of Mo and U isotope records. *Earth Sci. Rev.* **214**, 103506 (2021).
5. Barling, J., Arnold, G. L. & Anbar, A. D. Natural mass-dependent variations in the isotopic composition of molybdenum. *Earth Planet. Sci. Lett.* **193**, 447–457 (2001).
6. Siebert, C., Nägler, T. F., von Blanckenburg, F. & Kramers, J. D. Molybdenum isotope records as a potential new proxy for paleoceanography. *Earth Planet. Sci. Lett.* **211**, 159–171 (2003).
7. Siebert, C., McManus, J., Bice, A., Poulson, R. & Berelson, W. M. Molybdenum isotope signatures in continental margin marine sediments. *Earth Planet. Sci. Lett.* **241**, 723–733 (2006).
8. Poulson, R. L., Siebert, C., McManus, J. & Berelson, W. M. Authigenic molybdenum isotope signatures in marine sediments. *Geology* **34**, 617–620 (2006).
9. Goldberg, T. et al. Controls on Mo isotope fractionations in a Mn-rich anoxic marine sediment, Gullmar Fjord, Sweden. *Chem. Geol.* **296-297**, 73–82 (2012).
10. Kendall, B., Dahl, T. W. & Anbar, A. D. The stable isotope geochemistry of molybdenum. *Rev. Mineral. Geochem.* **82**, 683–732 (2017).
11. Chen, X. et al. Rise to modern levels of ocean oxygenation coincided with the Cambrian radiation of animals. *Nat. Commun.* **6**, 7142 (2015).
12. Dahl, T. W. et al. Devonian rise in atmospheric oxygen correlated to the radiations of terrestrial plants and large predatory fish. *Proc. Natl. Acad. Sci. USA* **107**, 17911–17915 (2010).
13. Xu, D. et al. Extensive sea-floor oxygenation during the early Mesoproterozoic. *Geochim. Cosmochim. Acta* **354**, 186–196 (2023).
14. Ye, Y. et al. Black shale Mo isotope record reveals dynamic ocean redox during the Mesoproterozoic Era. *Geochem. Perspect. Lett.* **18**, 16–21 (2021).
15. Qin, Z. et al. Molybdenum isotope-based redox deviation driven by continental margin euxinia during the early Cambrian. *Geochim. Cosmochim. Acta* **325**, 152–169 (2022).
16. Siebert, C., Scholz, F., Kuhnt, W. A new view on the evolution of seawater molybdenum inventories before and during the Cretaceous Oceanic Anoxic Event 2. *Chem. Geol.* **582**, 120399 (2021).
17. Neubert, N., Nägler, T. F. & Böttcher, M. E. Sulfidity controls molybdenum isotope fractionation into euxinic sediments: evidence from the modern Black Sea. *Geology* **36**, 775 (2008).
18. Nägler, T. F., Neubert, N., Böttcher, M. E., Dellwig, O. & Schnetger, B. Molybdenum isotope fractionation in pelagic euxinia: evidence from the modern Black and Baltic Seas. *Chem. Geol.* **289**, 1–11 (2011).
19. Eroglu, S., Scholz, F., Frank, M. & Siebert, C. Influence of particulate versus diffusive molybdenum supply mechanisms on the molybdenum isotope composition of continental margin sediments. *Geochim. Cosmochim. Acta* **273**, 51–69 (2020).
20. Scholz, F., McManus, J. & Sommer, S. The manganese and iron shuttle in a modern euxinic basin and implications for molybdenum cycling at euxinic ocean margins. *Chem. Geol.* **355**, 56–68 (2013).
21. Goto, K. T. et al. A framework for understanding Mo isotope records of Archean and Paleoproterozoic Fe- and Mn-rich sedimentary rocks: insights from modern marine hydrothermal Fe-Mn oxides. *Geochim. Cosmochim. Acta* **280**, 221–236 (2020).
22. Goldberg, T., Archer, C., Vance, D. & Poulton, S. W. Mo isotope fractionation during adsorption to Fe (oxyhydr)oxides. *Geochim. Cosmochim. Acta* **73**, 6502–6516 (2009).
23. Barling, J. & Anbar, A. D. Molybdenum isotope fractionation during adsorption by manganese oxides. *Earth Planet. Sci. Lett.* **217**, 315–329 (2004).
24. Wasylenki, L. E., Rolfe, B. A., Weeks, C. L., Spiro, T. G. & Anbar, A. D. Experimental investigation of the effects of temperature and ionic

strength on Mo isotope fractionation during adsorption to manganese oxides. *Geochim. Cosmochim. Acta* **72**, 5997–6005 (2008).
25. Wu F., Owens J. D., Tang L., Dong Y., Huang F. Vanadium isotopic fractionation during the formation of marine ferromanganese crusts and nodules. *Geochim. Cosmochim. Acta* **265**, 371–385 (2019).
26. Nakada, R., Takahashi, Y. & Tanimizu, M. Cerium stable isotope ratios in ferromanganese deposits and their potential as a paleo-redox proxy. *Geochim. Cosmochim. Acta* **181**, 89–100 (2016).
27. Rehkämper, M., Frank, M., Hein, J. R. & Halliday, A. Cenozoic marine geochemistry of thallium deduced from isotopic studies of ferromanganese crusts and pelagic sediments. *Earth Planet. Sci. Lett.* **219**, 77–91 (2004).
28. Wang, X., Planavsky, N. J., Reinhard, C. T., Hein, J. R. & Johnson, T. M. A Cenozoic seawater redox record derived from 238U/235U in ferromanganese crusts. *Am. J. Sci.* **316**, 64–83 (2016).
29. Ren, X., Li, H., Yan, S., Li, H. & Shi, X. Hydrogenetic and diagenetic controls on the specific surface area of polymetallic nodules in deep ocean basins. *Minerals* **13**, 1431 (2023).
30. Freymuth, H., Elliott, T., van Soest, M. & Skora, S. Tracing subducted black shales in the Lesser Antilles arc using molybdenum isotope ratios. *Geology* **44**, 987–990 (2016).
31. Wen, H. et al. Molybdenum isotopic records across the Precambrian-Cambrian boundary. *Geology* **39**, 775–778 (2011).
32. Baturin G. N. Manganese and molybdenum in phosphorites from the ocean. *Lithol. Mineral Res.* **37**, 412–428 (2002).
33. Bau, M. et al. Discriminating between different genetic types of marine ferro-manganese crusts and nodules based on rare earth elements and yttrium. *Chem. Geol.* **381**, 1–9 (2014).
34. Josso, P. et al. A new discrimination scheme for oceanic ferromanganese deposits using high field strength and rare earth elements. *Ore Geol. Rev.* **87**, 3–15 (2017).
35. Hein, J. R., Koschinsky, A. & Kuhn, T. Deep-ocean polymetallic nodules as a resource for critical materials. *Nat. Rev. Earth Environ.* **1**, 158–169 (2020).
36. Kashiwabara, T., Takahashi, Y., Tanimizu, M. & Usui, A. Molecular-scale mechanisms of distribution and isotopic fractionation of molybdenum between seawater and ferromanganese oxides. *Geochim. Cosmochim. Acta* **75**, 5762–5784 (2011).
37. Hein, J. R. et al. Critical metals in manganese nodules from the Cook Islands EEZ, abundances and distributions. *Ore Geol. Rev.* **68**, 97–116 (2015).
38. Algeo, T. J. & Li, C. Redox classification and calibration of redox thresholds in sedimentary systems. *Geochim. Et. Cosmochim. Acta* **287**, 8–26 (2020).
39. Froelich, P. N. et al. Early oxidation of organic matter in pelagic sediments of the eastern equatorial Atlantic: suboxic diagenesis. *Geochim. Cosmochim. Acta* **43**, 1075–1090 (1979).
40. Planavsky, N. J. et al. Evidence for oxygenic photosynthesis half a billion years before the Great Oxidation Event. *Nat. Geosci.* **7**, 283–286 (2014).
41. Morford, J. L. & Emerson, S. The geochemistry of redox sensitive trace metals in sediments. *Geochim. Cosmochim. Acta* **63**, 1735–1750 (1999).
42. Calvert, S. E. & Price, N. B. Geochemical variation in ferromanganese nodules and associated sediments from the Pacific Ocean. *Mar. Chem.* **5**, 43–74 (1977).
43. Cronan, D. S. Average abundances of Mn, Fe, Ni, Co, Cu, Pb, Mo, V, Cr, Ti and P in Pacific pelagic clays. *Geochim. Cosmochim. Acta* **33**, 1562–1565 (1969).
44. Canfield, D. E. & Thamdrup, B. Towards a consistent classification scheme for geochemical environments, or, why we wish the term 'suboxic' would go away. *Geobiology* **7**, 385–392 (2009).
45. Bekker, A. et al. Iron formation: the sedimentary product of a complex interplay among mantle, tectonic, oceanic, and biospheric processes. *Econ. Geol.* **105**, 467–508 (2010).
46. Maynard, J. B. The chemistry of manganese ores through time: a signal of increasing diversity of earth-surface environments. *Econ. Geol.* **105**, 535–552 (2010).
47. Tostevin, R. et al. Low-oxygen waters limited habitable space for early animals. *Nat. Commun.* **7**, 12818 (2016).
48. Feng, L. et al. A simple single-stage extraction method for Mo separation from geological samples for isotopic analysis by MC-ICP-MS. *J. Anal. At. Spectrom.* **35**, 145–154 (2020).
49. Nägler, T. F. et al. Proposal for an International Molybdenum Isotope Measurement Standard and Data Representation. *Geostand. Geoanal. Res.* **38**, 149–151 (2014).
50. Zhu, H.-G. et al. Validating the high-precision measurement of Mo isotopes at the 5 ng level using double spike MC-ICP-MS. *J. Anal. At. Spectrom.* **37**, 1063–1075 (2022).
51. Lawrence, M. G., Greig, A., Collerson, K. D. & Kamber, B. S. Rare Earth Element and Yttrium Variability in South East Queensland Waterways. *Aquat. Geochem.* **12**, 39–72 (2006).

Acknowledgements

This study was funded by the National Natural Science Foundation of China (42422304), Natural Science Foundation of Jiangsu Province (BK20240172), and the Laoshan Laboratory Project (No. LSKJ202203601). We thank Editors Joe Aslin and Carolina Ortiz Guerrero and three anonymous reviewers for their insightful comments and suggestions that improved this work. No permissions were required for sample collections.

Author contributions

G.-Y.W. designed the research. M.C., X.R., and X.S. collected the samples. M.C., X.R., Y.-B.L., T.L., G.-Y.W. and S.C. performed the elemental and isotopic analyses. M.C. wrote the draft, with substantial inputs from G.-Y.W., F.Z., X.R., X.S., H.-F.L., S.-z.S., and J.C. All authors contributed substantially to researching data for the article and the discussion of its content.

Competing interests

The authors declare no other competing interests, while F.Z. is an Editorial Board Member for Communications Earth & Environment, but was not involved in the editorial review of, nor the decision to publish this article.

Additional information

Supplementary information The online version contains supplementary material available at https://doi.org/10.1038/s43247-025-02571-z.

Correspondence and requests for materials should be addressed to Guang-Yi Wei.

Peer review information *Communications Earth and Environment* thanks and the other, anonymous, reviewer(s) for their contribution to the peer review of this work. Primary Handling Editors: Joe Aslin and Carolina Ortiz Guerrero. A peer review file is available.

Reprints and permissions information is available at http://www.nature.com/reprints

Publisher's note Springer Nature remains neutral with regard to jurisdictional claims in published maps and institutional affiliations.

Open Access This article is licensed under a Creative Commons Attribution-NonCommercial-NoDerivatives 4.0 International License, which permits any non-commercial use, sharing, distribution and reproduction in any medium or format, as long as you give appropriate credit to the original author(s) and the source, provide a link to the Creative Commons licence, and indicate if you modified the licensed material. You do not have permission under this licence to share adapted material derived from this article or parts of it. The images or other third party material in this article are included in the article's Creative Commons licence, unless indicated otherwise in a credit line to the material. If material is not included in the article's Creative Commons licence and your intended use is not permitted by statutory regulation or exceeds the permitted use, you will need to obtain permission directly from the copyright holder. To view a copy of this licence, visit http://creativecommons.org/licenses/by-nc-nd/4.0/.

© The Author(s) 2025